

NACA RM A53F12



0143360



TECH LIBRARY KAFB, NM

RESEARCH MEMORANDUM

9T49
CORRELATION BY THE HYPERSONIC SIMILARITY RULE OF PRESSURE
DISTRIBUTIONS AND WAVE DRAGS FOR MINIMUM-DRAG NOSE
SHAPES AT ZERO ANGLE OF ATTACK

By Leland H. Jorgensen

Ames Aeronautical Laboratory
Moffett Field, Calif.

Classification cancelled (or changed to *UNCLASSIFIED*)

By Authority of *NASA Tech Pub. Authorization* (Officer Authorized to Change)

By *L.H.J.*
NAME AND

.....
GRADE OF OFFICER MAKING CHANGE

..... *24 Mat. G.*
DATE

NATIONAL ADVISORY COMMITTEE
FOR AERONAUTICS

WASHINGTON
August 31, 1953

RECEIPT SIGNATURE
REQUIRED



NATIONAL ADVISORY COMMITTEE FOR AERONAUTICS

RESEARCH MEMORANDUM

CORRELATION BY THE HYPERSONIC SIMILARITY RULE OF PRESSURE

DISTRIBUTIONS AND WAVE DRAGS FOR MINIMUM-DRAG NOSE

SHAPES AT ZERO ANGLE OF ATTACK

By Leland H. Jorgensen

SUMMARY

The hypersonic similarity rule has been used to correlate pressure distributions and wave drags for minimum-drag nose shapes derived by von Kármán and Newton. The pressure distributions and wave drags have been computed by Van Dyke's second-order theory for various Mach number and fineness ratio combinations resulting in values of the similarity parameter (Mach number divided by fineness ratio) between 0.4 and 1.0. The computed results, presented as a function of the similarity parameter, have been confirmed by comparison with available experimental data. From analysis of the results, simple expressions for pressure distribution and wave drag in terms of the hypersonic similarity parameter have been developed.

Wave-drag results for both the Karman and Newtonian shapes are compared with each other and with results for cones and circular-arc tangent ogives. The Newtonian shapes have about 10 percent less wave drag than the Karman shapes for values of the similarity parameter of about 0.8. They also have 20 to 25 percent less wave drag than tangent ogives and 15 to 20 percent less wave drag than cones.

INTRODUCTION

The hypersonic similarity rule, derived by Tsien (ref. 1) and Hayes (ref. 2) provides the aerodynamicist with a practical tool which greatly reduces the work necessary to determine the aerodynamic properties of related bodies of revolution at supersonic Mach numbers and zero incidence. According to this rule, the hypersonic flow patterns about slender, pointed, affinely related bodies are similar, provided the values of the similarity parameter K (Mach number divided by fineness ratio) are equal.

[Redacted]

[Signature] - 22

Although the statement of the rule would indicate that its applicability might be limited to high supersonic Mach numbers and very slender bodies, recent studies (refs. 3 and 4) have shown the rule to be valid for correlating pressure distributions and wave drags for cones and tangent ogives, even for Mach numbers as low as approximately 1.5 and fineness ratios as small as 2. According to references 5 and 6, this rule has been shown to be applicable even for correlating wave drags of slightly blunt bodies.

With the assumption, therefore, that the hypersonic similarity rule is a valid tool for correlating results, an investigation was undertaken to study the pressure-distribution and wave-drag characteristics of two minimum-drag nose shapes, one derived by von Kármán (ref. 7) and the other by Newton (refs. 8 and 9). These shapes are of interest since both were theoretically optimized for minimum drag for the conditions of given length and diameter, and yet their profiles differ appreciably due to the diverse assumptions and pressure-velocity relationships employed in their derivations. Due to the use of slender-body theory in the derivation of the Kármán shape, one might expect the shape to have minimum drag only for high fineness ratios and low supersonic Mach numbers (or low values of K). In contrast, the Newtonian shape derived by use of Newton's law of resistance might be expected to exhibit less drag than the Kármán shape only at high supersonic Mach numbers (or high values of K). Since, by the hypersonic similarity rule, Mach number and fineness ratio can be combined into a single parameter, the wave drags of these shapes may be conveniently compared on a plot showing the variation of the wave-drag function with the similarity parameter. Such a plot for comparing the wave drag of these shapes was made for a previous investigation (ref. 5) but has been extended and more completely analyzed for this investigation. Wave-drag comparisons have been made over a similarity-parameter range of from about 0.4 to 1.0. Since only a small amount of experimental data exists for the Kármán and Newtonian shapes, pressure-distribution and wave-drag values for this study were computed using second-order theory (ref. 10).

In the course of studying the pressure-distribution and wave-drag curves, it was found that simple equations for pressure distribution and wave drag in terms of the similarity parameter could be written for each shape, thus enabling rapid calculation of these characteristics for many practical combinations of Mach number and fineness ratio. The purpose of this report, in addition to presenting and comparing pressure-distribution and wave-drag characteristics for the Kármán and Newtonian nose shapes, is to present these simple equations and show the manner in which they were determined.

SYMBOLS

A base area of nose shape

a pressure-ratio intercepts at $x/l = 1$ from the pressure-ratio curves for the Kármán shapes, $\left(\frac{p}{p_0}\right)_{x/l=1}$

b pressure-coefficient intercepts at $x/l = 1$ from the pressure-coefficient curves for the Newtonian shapes, $\left(\frac{p-p_0}{p_0}\right)_{x/l=1}$

c_D wave-drag coefficient, $\frac{\text{wave drag}}{q_0 A}$

d base diameter

K similarity parameter, $\frac{M_0}{l/d}$

l nose length

l/d nose fineness ratio

M_0 free-stream Mach number

m slope pressure-ratio curves for the Kármán shapes,
$$\frac{d \log_{10}(p/p_0)}{d \log_{10}(x/l)}$$

n slope of pressure-coefficient curves for the Newtonian shapes,
$$\frac{d \log_{10}[(p - p_0)/p_0]}{d \log_{10}(x/l)}$$

p local static pressure

p_0 free-stream static pressure

q_0 free-stream dynamic pressure

r local radius

r_b base radius

x longitudinal coordinate measured from vertex

x_c	longitudinal distance from vertex of basic nose profile to point of tangency of assumed conical tip with basic nose profile
θ	cone half angle
γ	ratio of specific heats of air, taken as 1.40
φ	$\cos^{-1} \left(1 - \frac{2x}{l} \right)$

SCOPE AND PROCEDURE

Profiles

Nondimensional plots of the profiles of the Kármán, the true Newtonian, and an approximated Newtonian minimum-drag nose shape are compared in figure 1. Although there is considerable difference between the Kármán and the true Newtonian shape, there is very little difference between the true Newtonian and the approximated Newtonian, or 3/4-power shape, which has been used in previous studies (refs. 5, 6, 9, and 11). Since the defining equation for the approximated shape offers great simplification in the calculation of pressure distribution and wave drag, it has been used in preference to the unwieldly true Newtonian expression (given in refs. 8 and 9). The profile equations used for this investigation, in the notation of the present report, are as follows:

For the Kármán shapes,

$$r = \frac{r_b}{\sqrt{\pi}} \sqrt{\varphi - \frac{1}{2} \sin 2\varphi} \quad (1)$$

where

$$\varphi = \cos^{-1} \left(1 - \frac{2x}{l} \right)$$

For the Newtonian shapes,

$$r = r_b \left(\frac{x}{l} \right)^{3/4} \quad (2)$$

Theoretical Pressure-Distribution and Wave-Drag Calculations

Van Dyke's second-order theory (ref. 10) was used to calculate pressure distributions and wave drags for the nose shapes considered. For

similarity parameters between 0.4 and 1.0, calculations were made for the Mach number and fineness ratio combinations listed in the following tables:¹

Kármán shapes				Newtonian shapes			
K	M ₀	l/d	x _c /l	K	M ₀	l/d	x _c /l
0.429	3	7	0.024	0.429	3	7	0.038
.500	1.5	3	.024	.500	1.5	3	.019
.500	1.5	3	.048	.500	1.5	3	.038
.600	3	5	.024	.500	1.5	3	.076
.600	3	5	.048	.500	4.5	9	.038
.667	2	3	.024	.600	3	5	.038
.750	2.25	3	.024	.667	2	3	.038
.857	2.57	3	.048	.750	5.25	7	.038
.857	6	7	.048	.857	6	7	.038
.922	6.45	7	.048	1.000	3	3	.038
				1.000	7	7	.038

The procedure followed in the calculations was that given in reference 10, wherein the approximate boundary conditions at the body surface are used in the calculation of the perturbation velocities, and the exact pressure relationship is used to evaluate the pressure coefficients. The theory is strictly applicable only for sharp-nosed bodies of revolution in the Mach number range bounded by the Mach number for shock-wave detachment and the Mach number at which the Mach cone is tangent to the nose vertex.² As both the Kármán and Newtonian shapes have mathematically infinite slopes at their vertices (yet for most practical purposes are sharp), a small conical tip tangent to the true profile of each nose must be assumed to enable use of the theory. To test the effect of this assumed tip modification, pressure distributions were calculated for Kármán and Newtonian shapes with progressively shorter conical tips. The results, shown in figure 2, indicate that the assumption of these conical tips has little, if any, effect on the major portions of the pressure distributions. However, to minimize any effect of nose tip modification on pressure distribution, the point of tangency of the conical tip with the true contour (x_c/l) was always taken at less than 5 percent of the body length. If desired, the pressure coefficients which would exist at the vertices ($x/l = 0$) of the blunt nose shapes could be computed by

¹The x_c/l values listed in the tables are the longitudinal distances from the vertices of the basic shapes to the points of tangency of conical tips assumed to permit solution with second-order theory.

²In order to use the tables of reference 10, the ratio of semivertex angle to Mach angle must not be greater than 0.94.

the use of Rayleigh's pitot-tube equation. These calculations were omitted for this investigation, since the resulting pressure coefficients would be functions of Mach number only and obviously could not satisfy the hypersonic similarity rule. However, even though the pressure coefficients at the vertices are omitted and those very near the vertices may be somewhat in error, the wave-drag results are affected very little when the wave-drag equation,

$$C_D \frac{q_0}{p_0} = \frac{2}{r_b^2} \int_0^{r_b} \left(\frac{p - p_0}{p_0} \right) r dr$$

is graphically integrated by plotting $r(p-p_0)/p_0$ as a function of r , and a smooth curve is faired to the origin.

RESULTS AND DISCUSSION

Pressure Distributions

Correlation and comparison with experiment. - In figures 3(a) and (b) all the theoretical pressure-distribution results for the various Mach number and fineness ratio combinations considered have been plotted with K as a parameter. These figures help substantiate the assumption of the validity and usefulness of the hypersonic similarity rule as a tool for correlating pressure distributions for the shapes considered. The validity of the rule is demonstrated for several values of similarity parameter K . For example, at $K = 0.857$ in figure 3(a), the pressure distribution for a fineness ratio 7 Kármán shape at Mach number 6 agrees well with that for a fineness ratio 3 Kármán shape at Mach number 2.57, the computed points for each solution falling very close to the mean faired curve. Likewise, in figure 3(b) additional checks are shown for Newtonian shapes for similarity parameters of 0.5 and 1.0.

At $K = 0.667$ ($M_0 = 2$, $l/d = 3$) the theoretical pressure-distribution curves for both the Kármán and Newtonian shapes have been verified by the results of experimental pressure-distribution tests conducted in the Ames 1- by 3-foot supersonic wind tunnel No. 1. The $K = 0.667$ curves of figures 3(a) and 3(b) (with the computed theoretical points omitted) are compared in figure 4 with the experimental results. The agreement between the theoretical curves and the experimental points is excellent and lends support to the use of second-order theory for this investigation.

Analytical expressions for pressure distribution. - Analysis of the data of figure 3 has revealed that for each family of nose shapes, a simple equation may be written for the variation of pressure coefficient with x/l and K . When pressure ratios p/p_0 for the Kármán shapes and pressure coefficients $(p-p_0)/p_0$ for the Newtonian shapes are plotted as a function of x/l on logarithmic coordinates, the resulting curves are linear over most of the nose length. (See fig. 5.) Exceptions to this linearity exist only for values of x/l greater than about 0.7 for the Kármán shapes and less than about 0.05 for both families of shapes. The equations for the linear curves may be expressed in exponential form as follows:

For the Kármán shapes,

$$\frac{p}{p_0} = a \left(\frac{x}{l} \right)^m \quad (3)$$

For the Newtonian shapes,

$$\frac{p - p_0}{p_0} = b \left(\frac{x}{l} \right)^n \quad (4)$$

where m and n represent the slopes of the curves shown in figures 5(a) and 5(b), and a and b represent the intercepts at $x/l = 1.0$. From plots of the variation of m and n with K (fig. 6(a)), it was found that

$$m = -0.399 K + 0.065 \quad (5)$$

and

$$n = -0.416 \quad (6)$$

From logarithmic plots of the variation of a and b with K (fig. 6(b)), it was also observed that

$$a = 1.080 K^{0.093} \quad (7)$$

and

$$b = 0.305 K^{1.683} \quad (8)$$

Thus, expressions for pressure coefficient as a function of x/l and K may be written as follows:

For the Kármán shapes ($0.05 < \frac{x}{l} < 0.7$),

$$\frac{p - p_0}{p_0} = \frac{p}{p_0} - 1 = 1.080 K^{0.683} \left(\frac{x}{l}\right)^{-0.399} K + 0.065 - 1 \quad (9)$$

For the Newtonian shapes³ ($0.05 < \frac{x}{l} < 1.0$),

$$\frac{p - p_0}{p_0} = 0.305 K^{1.683} \left(\frac{x}{l}\right)^{-0.416} \quad (10)$$

At least within the similarity-parameter limits investigated (and for M_∞ 's and l/d 's of the order of those used herein), pressure-distribution values for the Kármán and Newtonian nose shapes may be computed from equations (9) and (10), respectively. Although equation (9) is not applicable for x/l 's greater than 0.7 for the Kármán shapes, the pressure distributions past this point may be estimated with the aid of figure 3(a). The possibility that equation (10) for the Newtonian shapes may be used to compute pressure distributions for even higher values of K than one is intimated by the good agreement, shown later, between computed wave-drag values and experimental results for K 's to about 1.7.

Wave Drag

Analytical expressions for wave drag. - The wave-drag coefficients which were calculated from the theoretical pressure distributions of figure 3 are presented in figure 7, which shows the variation of the wave-drag function $C_D(q_0/p_0)$ with the similarity parameter K . For both the Kármán and Newtonian shapes, curves have been faired through the computed points. For the Kármán shapes (fig. 7(a)), the variation of the wave-drag function with the similarity parameter is linear (for the limits of K investigated), and the resulting expression is

$$C_D \frac{q_0}{p_0} = 0.6 K - 0.16 \quad (11)$$

For the Newtonian shapes (fig. 7(b)), the variation of the wave-drag function with the similarity parameter is not linear but may be expressed by

$$C_D \frac{q_0}{p_0} = 0.422 K^{1.683} \quad (12)$$

³It is of interest to note that this expression is of the same form as $(p-p_0)/p_0 = 0.197 K^2 (x/l)^{-0.5}$, which results from use of the Newtonian pressure relationship for slender bodies, $(p-p_0)/q_0 = 2(dr/dx)^2$.

This equation was analytically derived with the aid of the previously developed pressure-coefficient expression for the Newtonian shapes (eq. (10)).

Comparison of theoretical and experimental wave-drag results. - In figure 8 theoretical wave-drag curves resulting from the use of equations (11) and (12) are compared with wave-drag results obtained by subtracting calculated values of skin-friction drag from previously published experimental foredrag data (refs. 5, 9, and 11). These foredrag data were obtained from wind-tunnel tests of minimum-drag nose shapes of fineness ratios 3 and 5 at Mach numbers between 1.44 and 5.00. Since for the models tested the boundary-layer flow was laminar and the skin-friction drag was generally a small portion of the foredrag, the skin-friction drag, which has been subtracted from the published foredrag, was computed by the Blasius formula for flat-plate incompressible boundary-layer flow. Use of a more refined method to include the effects of body shape and compressibility was not considered necessary.

In order to make drag comparisons over the complete similarity-parameter range for which there is experimental data available, the theoretical wave-drag curves (eqs. (11) and (12)) have been extended past the K limits for which second-order-theory calculations have been made. (Compare, e.g., figs. 7 and 8.) It is evident from figure 8 that, even for these extended values of K , there is good agreement between the theoretical and experimental wave-drag results, although there appears to be some scatter in the experimental data. Thus, it may be expected that equations (11) and (12) can be reliably used for the calculation of wave drag for Kármán and Newtonian nose shapes within the K limits for which experimental confirmation has been shown ($0.41 < K < 1.02$ for Kármán shapes and $0.41 < K < 1.67$ for Newtonian shapes). Without further investigation, however, it would be inadvisable to use these equations for Mach numbers less than about 1.5 and for fineness ratios less than about 3.

Wave-drag comparisons between Kármán shapes, Newtonian shapes, cones, and tangent ogives. - In figure 9 curves showing the variation of the wave-drag function with the similarity parameter are compared for Kármán shapes, Newtonian shapes, cones, and circular-arc tangent ogives. The drag curves for the Kármán and Newtonian shapes are the same as those shown in figure 8, and the drag curves for the cones and tangent ogives are from references 3 and 4, respectively. The drag curve for cones (computed on the basis of the Taylor-Maccoll exact theory) and the drag curve for tangent ogives (computed by the method of characteristics) have both recently been experimentally verified (ref. 6).

As mentioned in the report introduction, the wave drag of a Newtonian shape might be expected to be less than that of a Kármán shape for high values of K . The results of this investigation and of reference 5 show that even for similarity parameters as low as 0.5 the wave drag of a

Newtonian shape is less than that of a Kármán shape. A designer confronted with the problem of choosing a nose shape for a given length and diameter should, of course, weigh the wave-drag savings which a Newtonian shape may offer against the 25 percent greater nose volume which a Karman shape offers. Although for the similarity-parameter range investigated the wave drag of a Newtonian shape is at most 10 percent less than that of a Kármán shape, it is 20 to 25 percent less than that of a tangent ogive and 15 to 20 percent less than that of a cone.

CONCLUSIONS

The hypersonic similarity rule has been used to correlate pressure distributions and wave drags for Kármán and Newtonian nose shapes over the similarity-parameter range from about 0.4 to 1.0. An analysis of the correlated results has led to the following conclusions:

1. For each family of shapes, simple equations for pressure distribution and wave drag may be written:

For the Kármán shapes,

$$\frac{p - p_0}{p_0} = 1.080 K^{0.093} \left(\frac{x}{l}\right)^{-0.398} K + 0.065 - 1 \quad (0.05 < \frac{x}{l} < 0.7)$$

and

$$C_D \frac{q_0}{p_0} = 0.6 K - 0.16$$

For the Newtonian shapes,

$$\frac{p - p_0}{p_0} = 0.305 K^{1.688} \left(\frac{x}{l}\right)^{-0.416} \quad (0.05 < \frac{x}{l} < 1.0)$$

and

$$C_D \frac{q_0}{p_0} = 0.422 K^{1.688}$$

where p is local static pressure; p_0 and q_0 are free-stream static and dynamic pressures, respectively; C_D is wave-drag coefficient based on base area; K is the similarity parameter, $M_\infty(l/d)$; and x/l is the longitudinal coordinate from the vertex divided by the nose length.

2. The Newtonian shapes have less wave drag than the Kármán shapes of the same fineness ratio for values of similarity parameter between 0.5 and 1.0.

3. Both Kármán and Newtonian shapes have less wave drag than either cones or circular-arc tangent ogives of the same fineness ratio, the wave drag of a Newtonian shape being 20 to 25 percent less than that of a tangent ogive and 15 to 20 percent less than that of a cone.

Ames Aeronautical Laboratory
National Advisory Committee for Aeronautics
Moffett Field, Calif., June 12, 1953

REFERENCES

1. Tsien, Hsue-Shen: Similarity Laws of Hypersonic Flows. *Jour. Math. and Phys.*, vol. 25, no. 3, Oct. 1946.
2. Hayes, Wallace D.: On Hypersonic Similitude. *Quart. Appl. Math.*, vol. V, no. 1, Apr. 1947.
3. Ehret, Dorris M., Rossow, Vernon J., and Stevens, Victor I.: An Analysis of the Applicability of the Hypersonic Similarity Law to the Study of Flow About Bodies of Revolution at Zero Angle of Attack. NACA TN 2250, 1950.
4. Rossow, Vernon J.: Applicability of the Hypersonic Similarity Rule to Pressure Distributions Which Include the Effects of Rotation for Bodies of Revolution at Zero Angle of Attack. NACA TN 2399, 1951. (Extension of NACA TN 2250)
5. Perkins, Edward W., and Jorgensen, Leland H.: Investigation of the Drag of Various Axially Symmetric Nose Shapes of Fineness Ratio 3 for Mach Numbers from 1.24 to 3.67. NACA RM A52E28, 1952.
6. Neice, Stanford E., and Wong, Thomas J.: An Experimental Investigation of the Applicability of the Hypersonic Similarity Law to Bodies of Revolution. NACA RM A52K07, 1953.
7. von Kármán, Th.: The Problems of Resistance in Compressible Fluids. *Reale Accad. d'Italia, Roma*, vol. XIV, 1936, pp. 222-276. (Fifth Volta Congress held in Rome, Sept. 30 - Oct. 6, 1935).
8. Newton, Isaac: *Principia* - Motte's Translation Revised. Univ. of Calif. Press, 1946, pp. 333, 657-661.

9. Eggers, A. J., Dennis, David H., and Resnikoff, Meyer M.: Bodies of Revolution for Minimum Drag at High Supersonic Airspeeds. NACA RM A51K27, 1952.
10. Van Dyke, Milton D.: Practical Calculation of Second-Order Supersonic Flow Past Nonlifting Bodies of Revolution. NACA TN 2744, 1952.
11. Dennis, David H., and Cunningham, Bernard E.: Forces and Moments on Pointed and Blunt-Nosed Bodies of Revolution at Mach Numbers From 2.75 to 5.00. NACA RM A52E22, 1952.

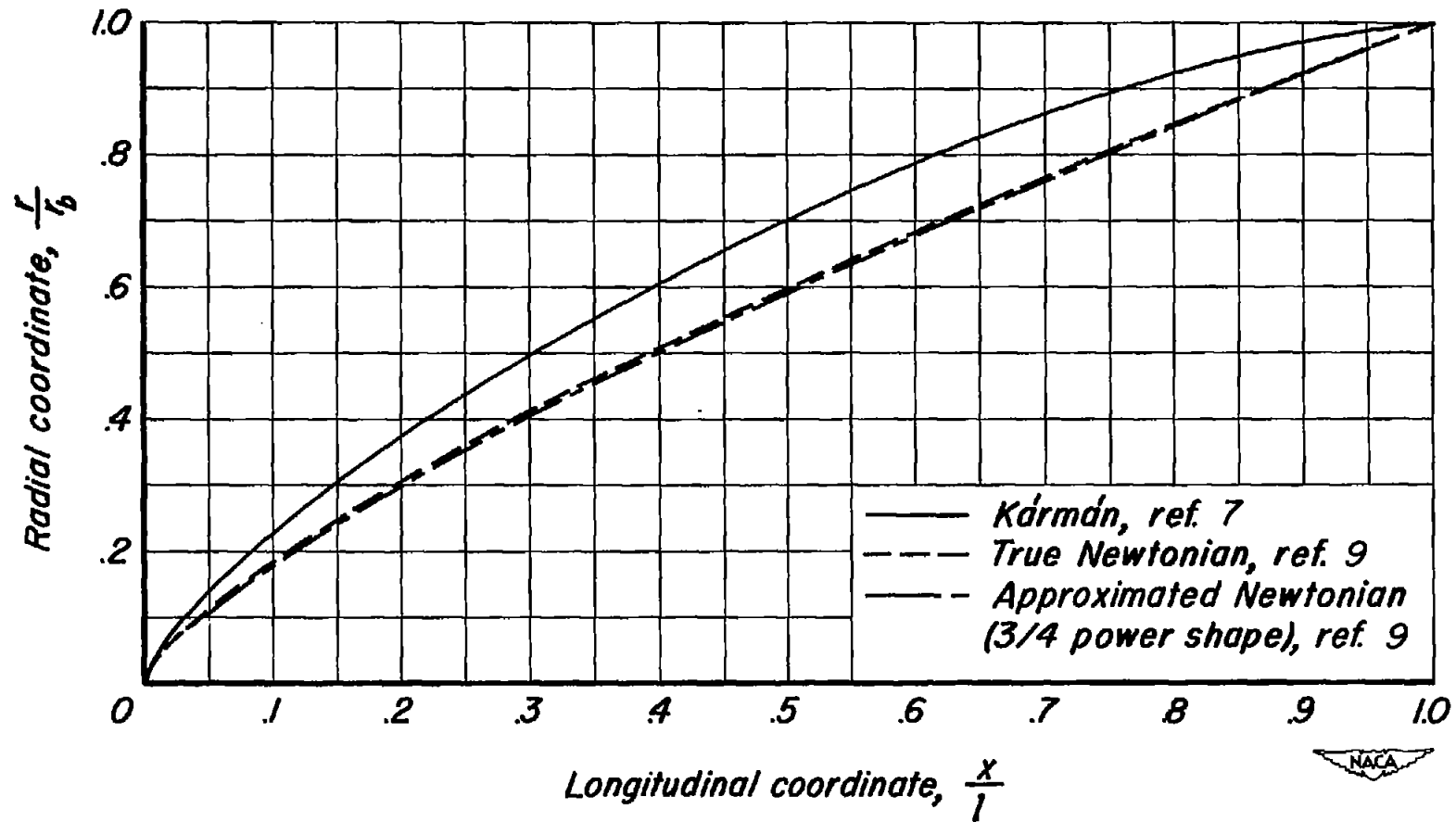


Figure 1.—Comparison of profiles of minimum-drag noses for given length and base diameter.

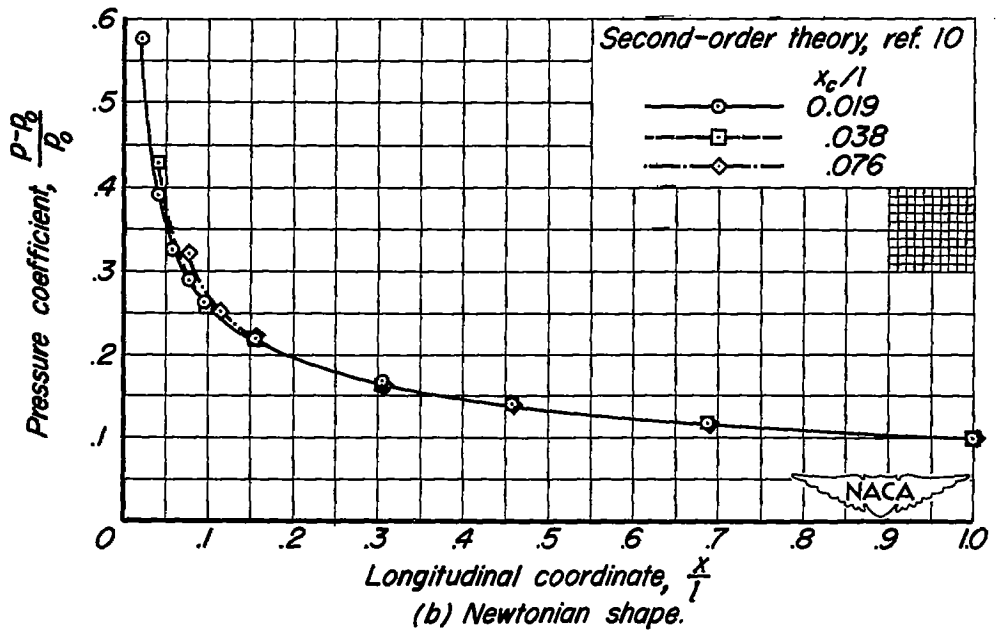
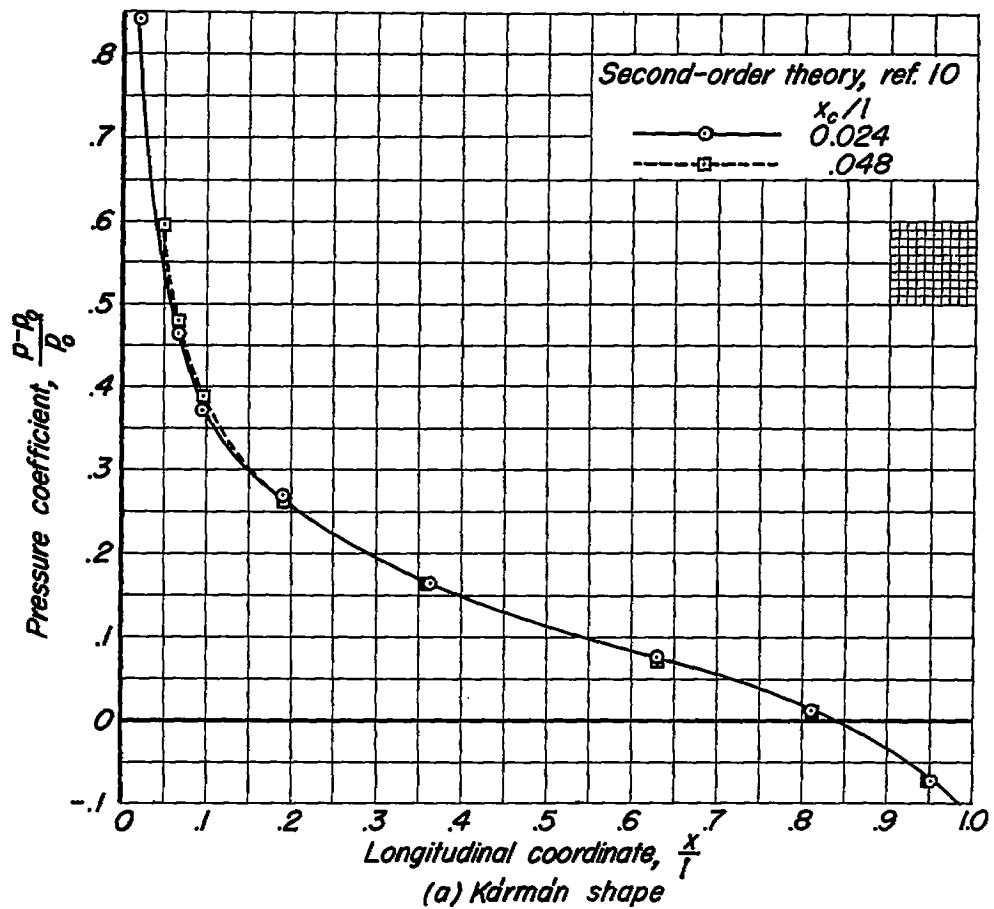


Figure 2. - Effect of conical tip modifications on the pressure distributions.
($l/d = 3$, $M_0 = 1.5$)

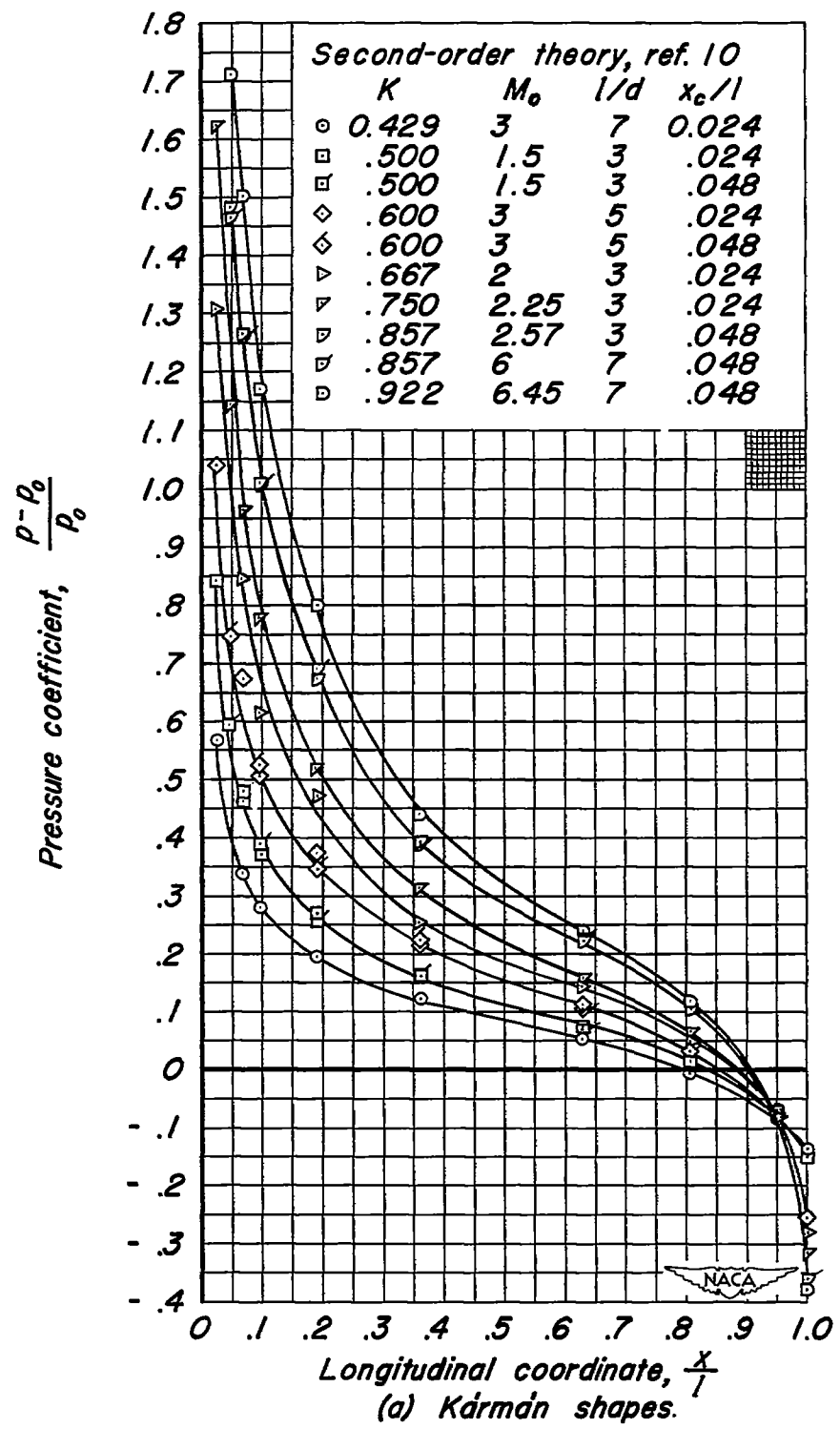


Figure 3.- Theoretical pressure distributions for various values of similarity parameter K .

~~CONTINUATION~~

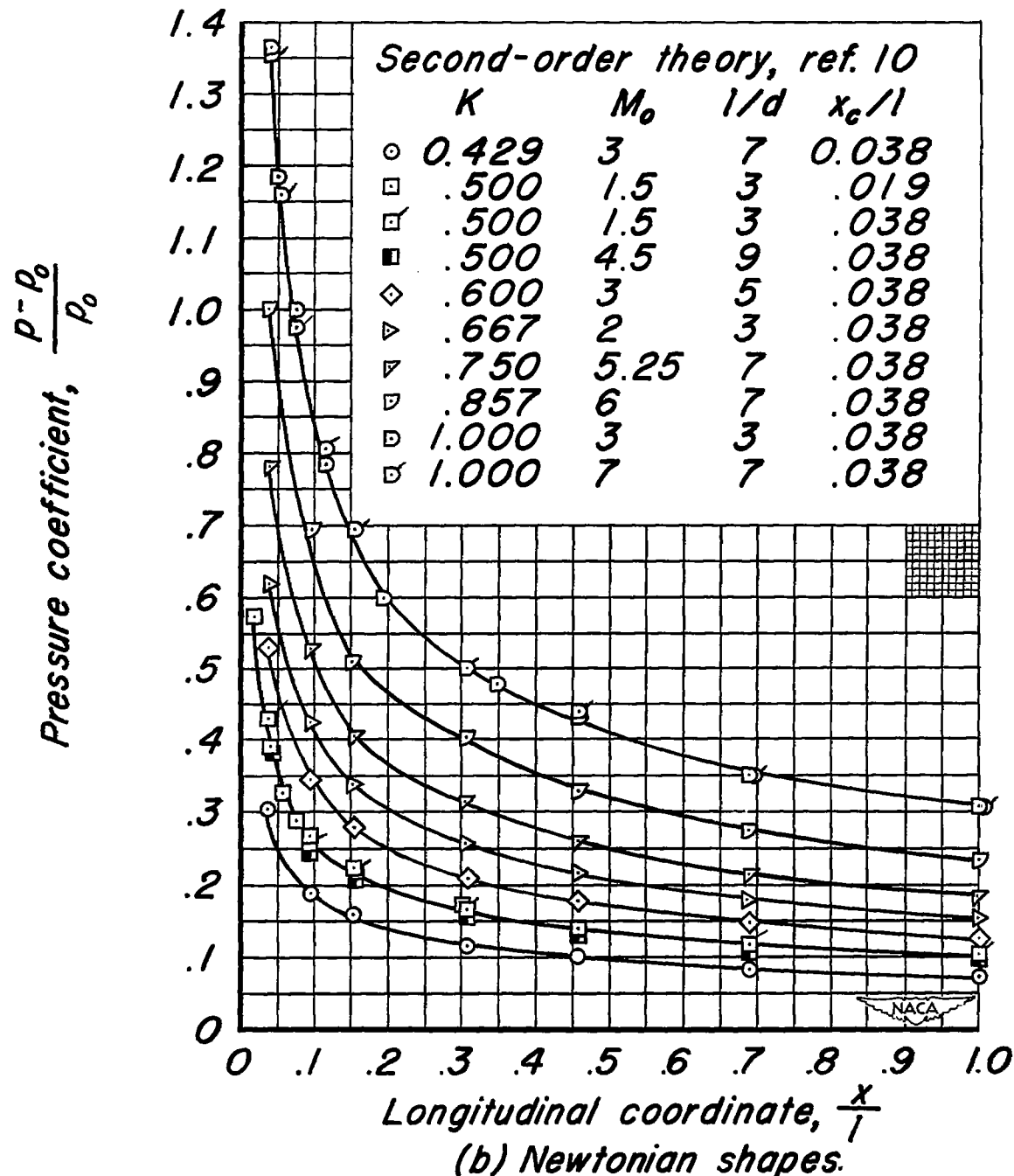


Figure 3.- Concluded.

~~CONFIDENTIAL~~

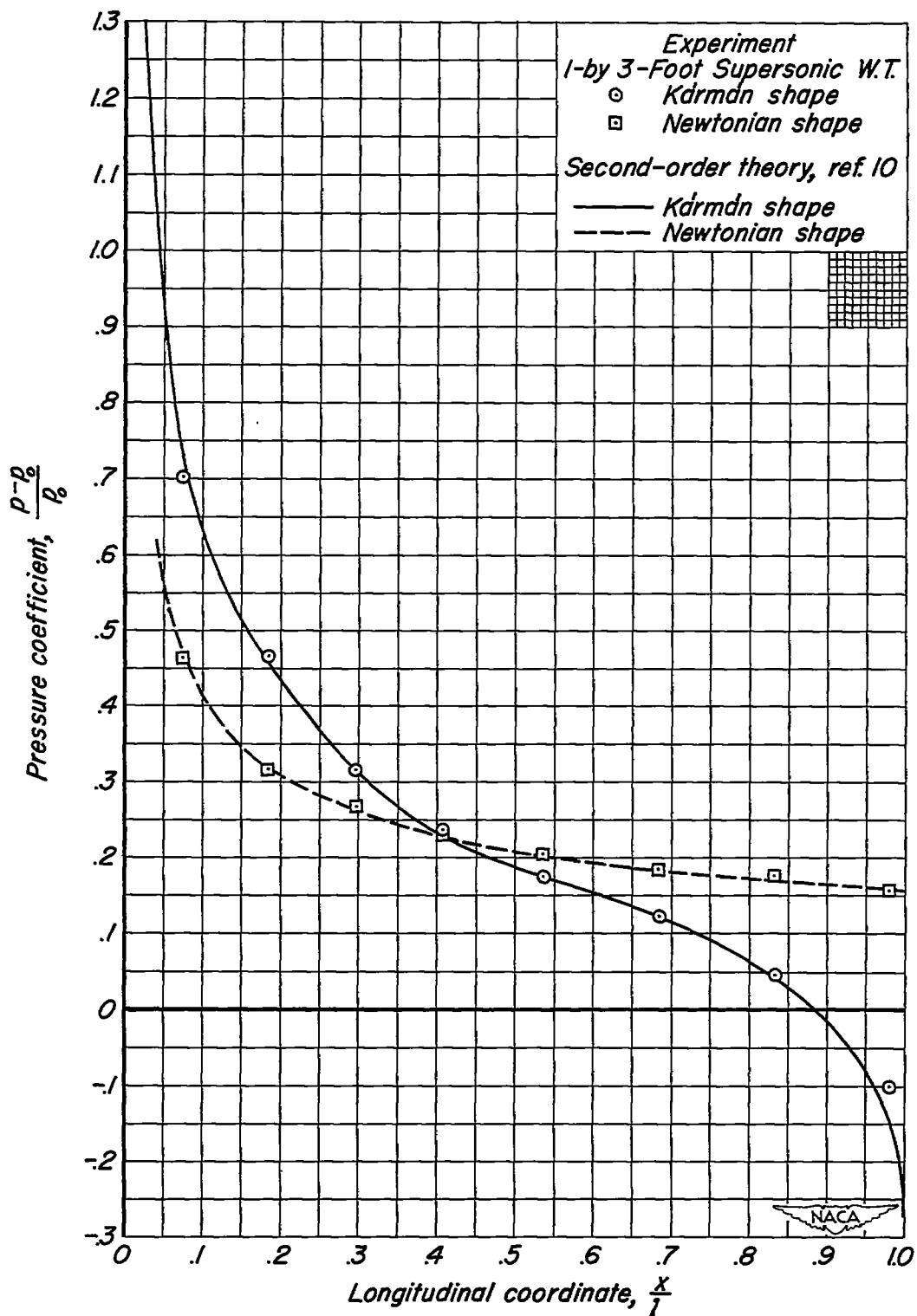


Figure 4.-Comparison of experimental and theoretical pressure distributions.
($l/d = 3, M_0 = 2, K = 0.667$)

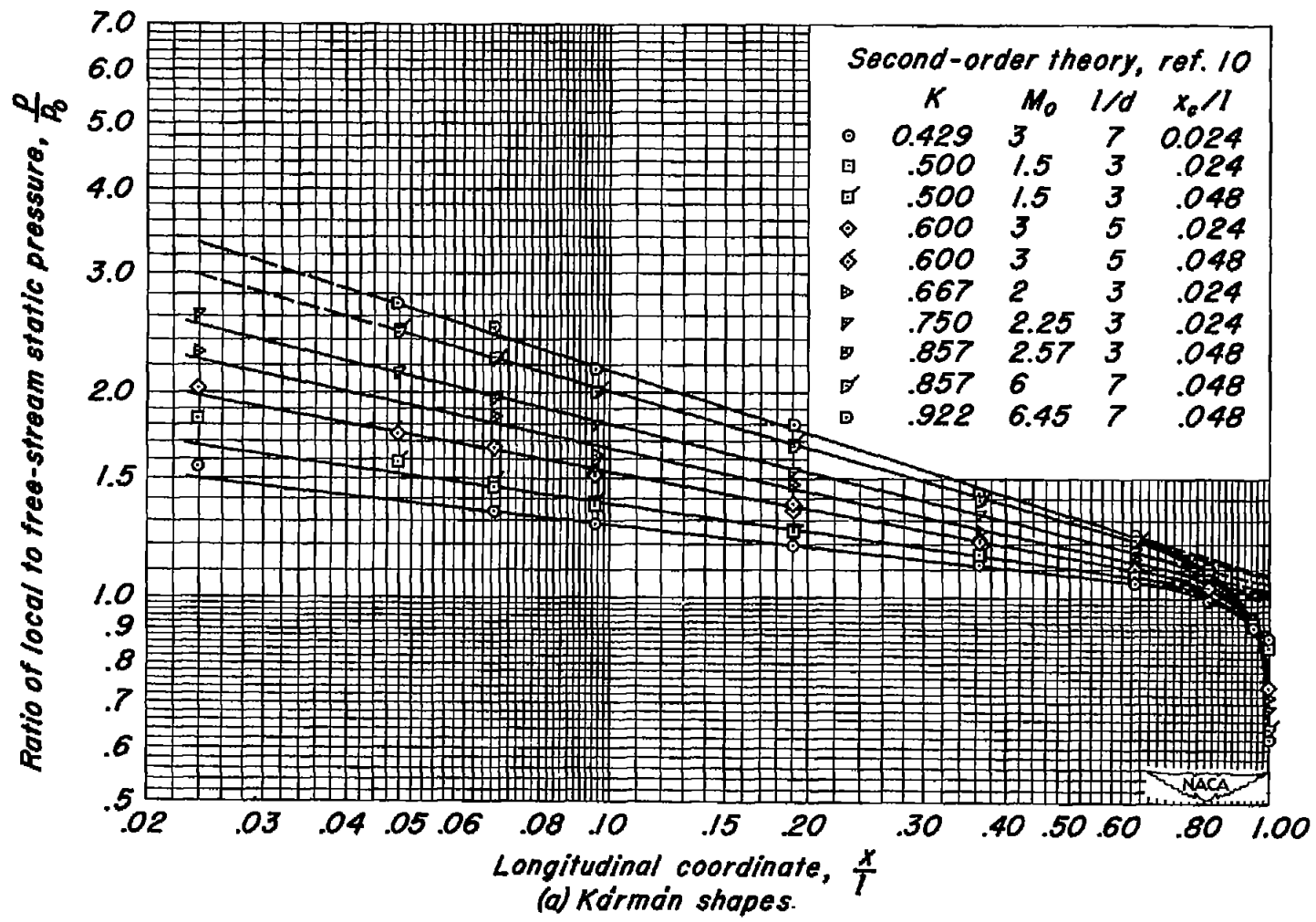
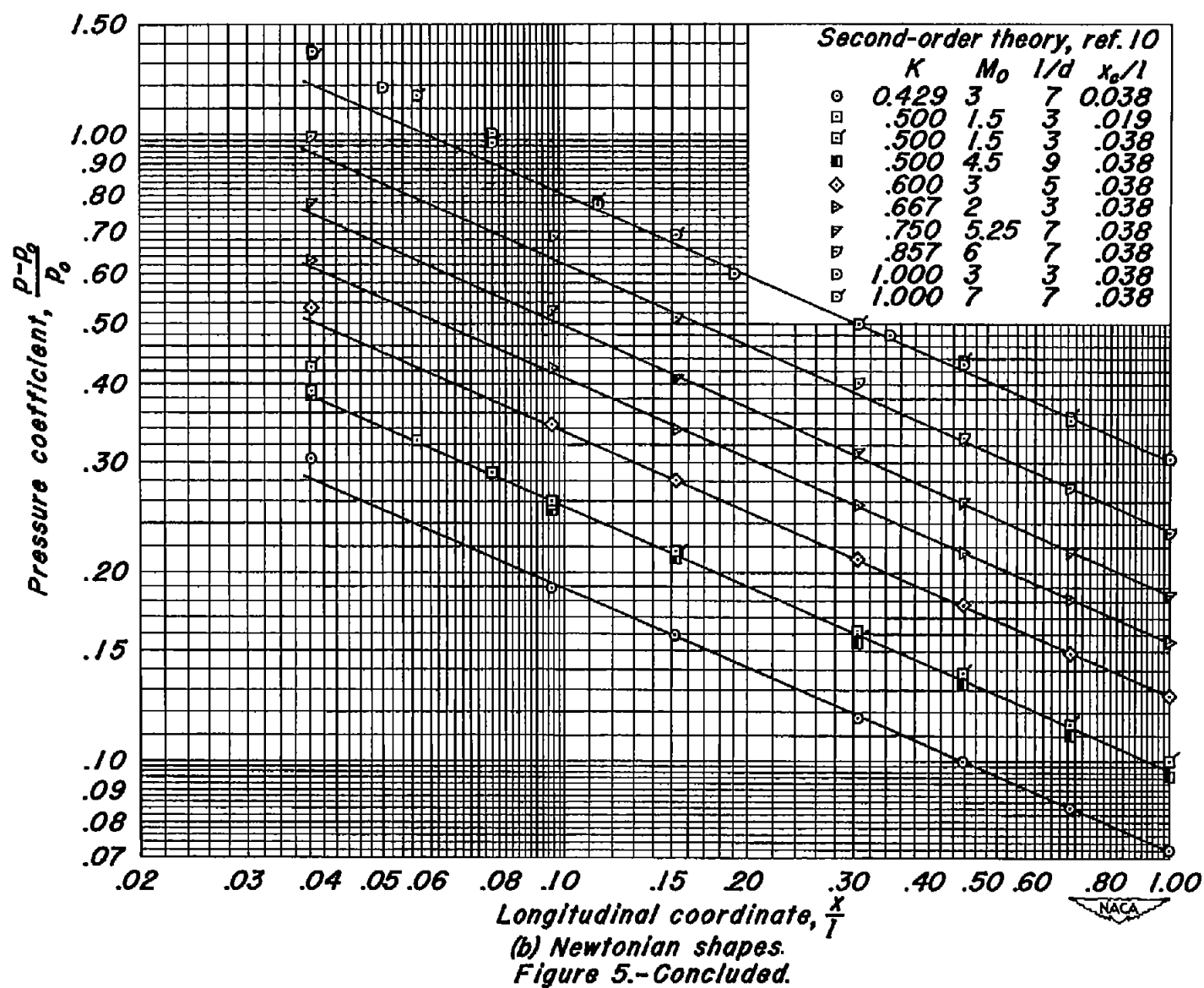


Figure 5.—Logarithmic plots of the theoretical pressure distributions for various values of similarity parameter K .



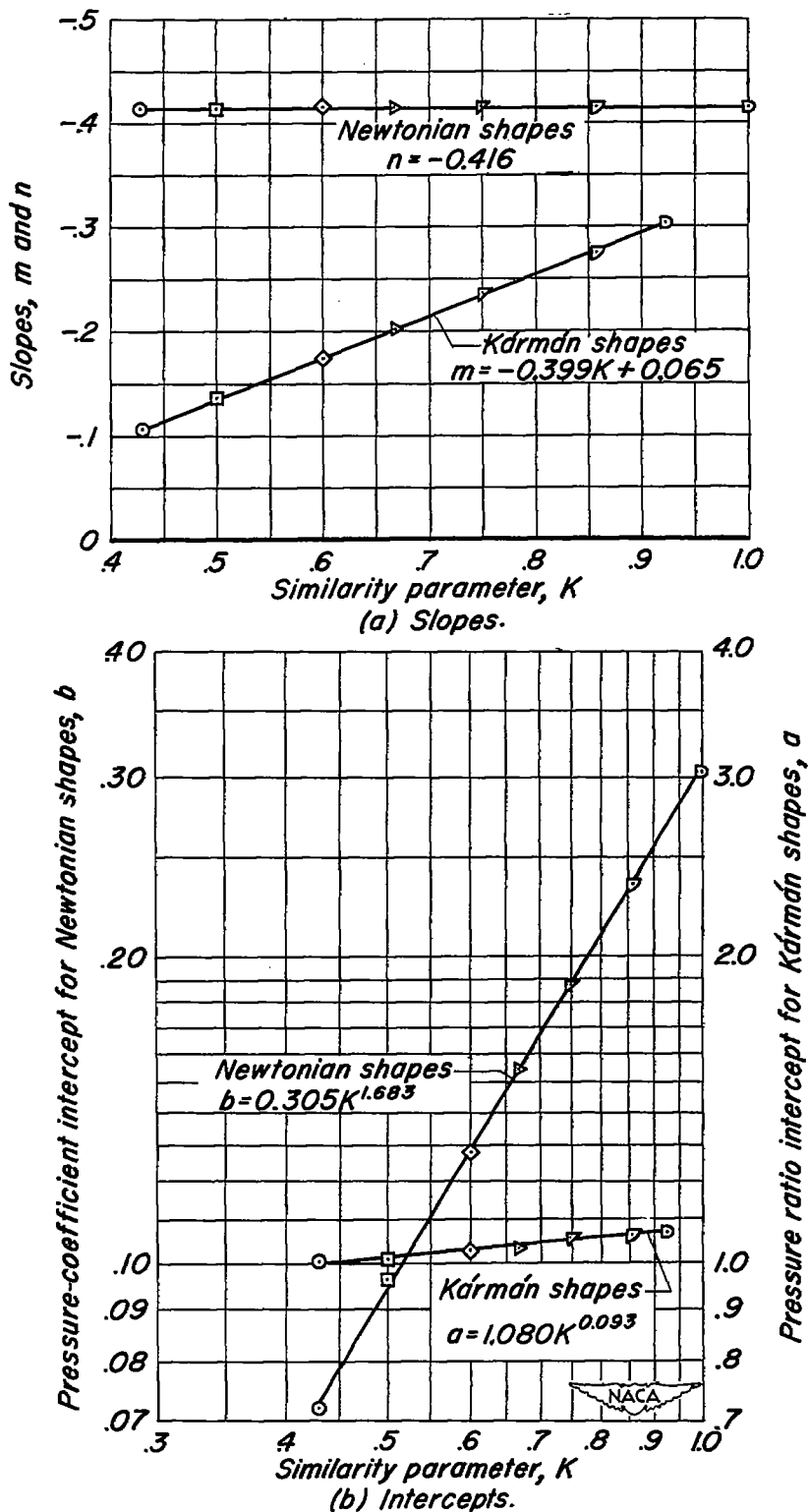


Figure 6.- Variation with similarity parameter K of the slopes and intercepts ($x/l=1$) of the pressure distributions of figure 5.

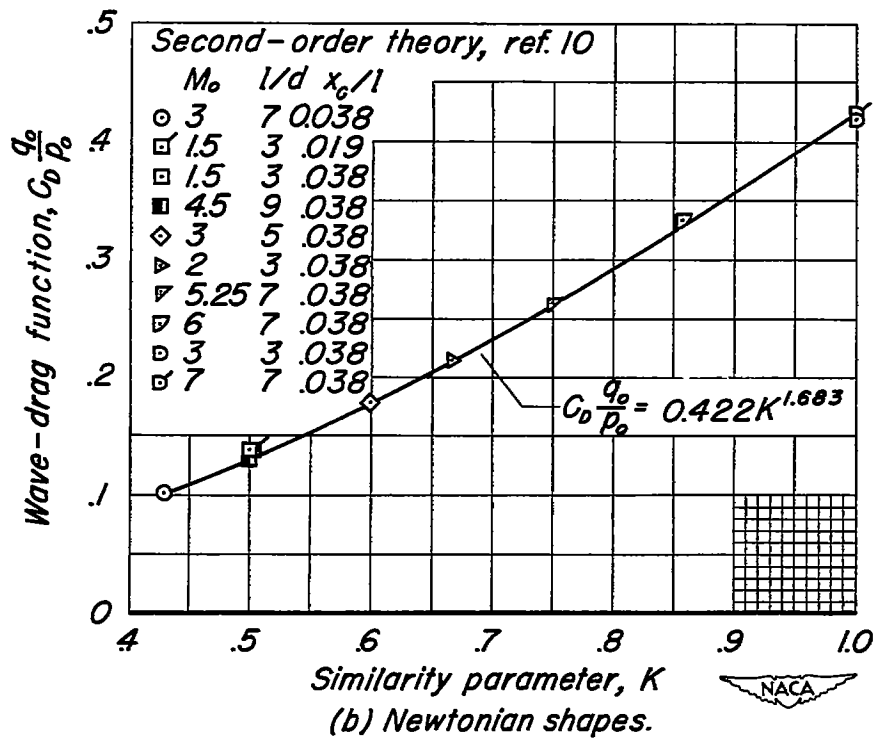
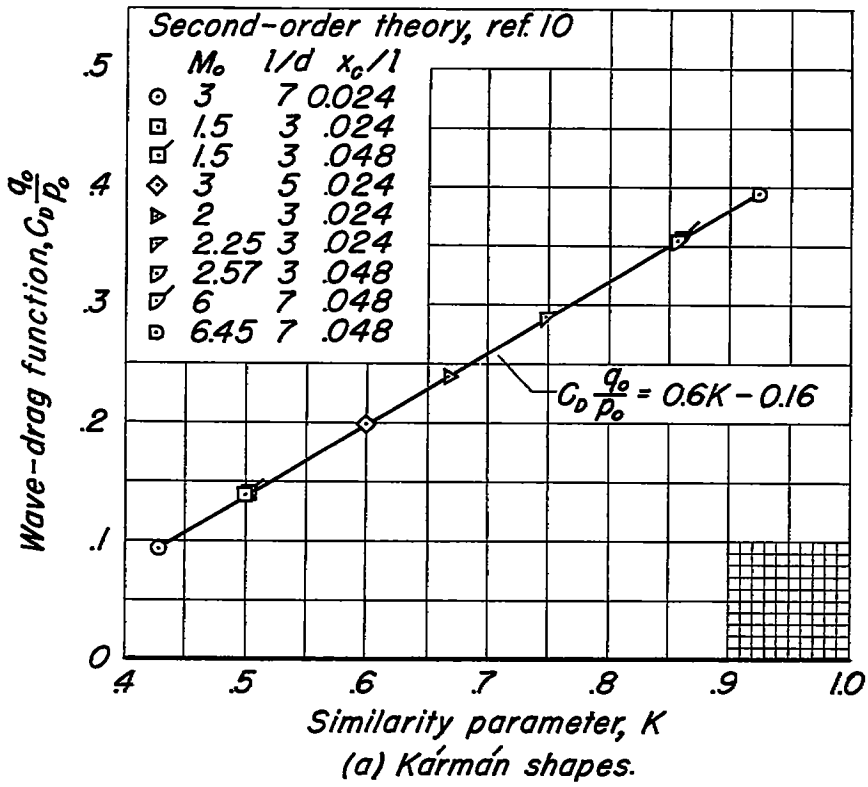


Figure 7-Theoretical variation of wave-drag function $C_D \frac{q_\infty}{\rho_0}$ with similarity parameter K .

~~CONFIDENTIAL~~

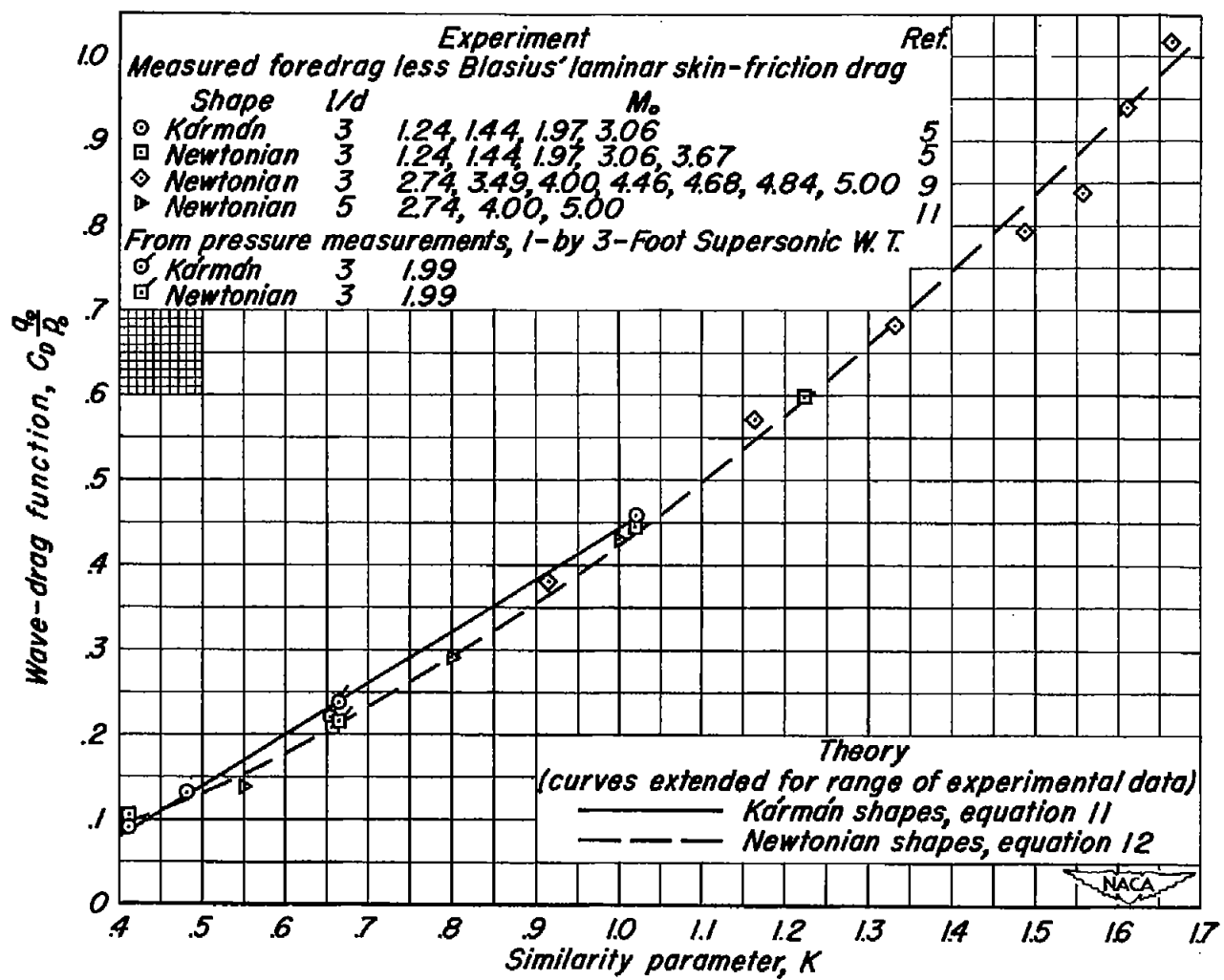


Figure 8.- Comparison of the experimental and theoretical variations of wave-drag function $C_D \frac{q_0}{\rho_0}$ with similarity parameter K .

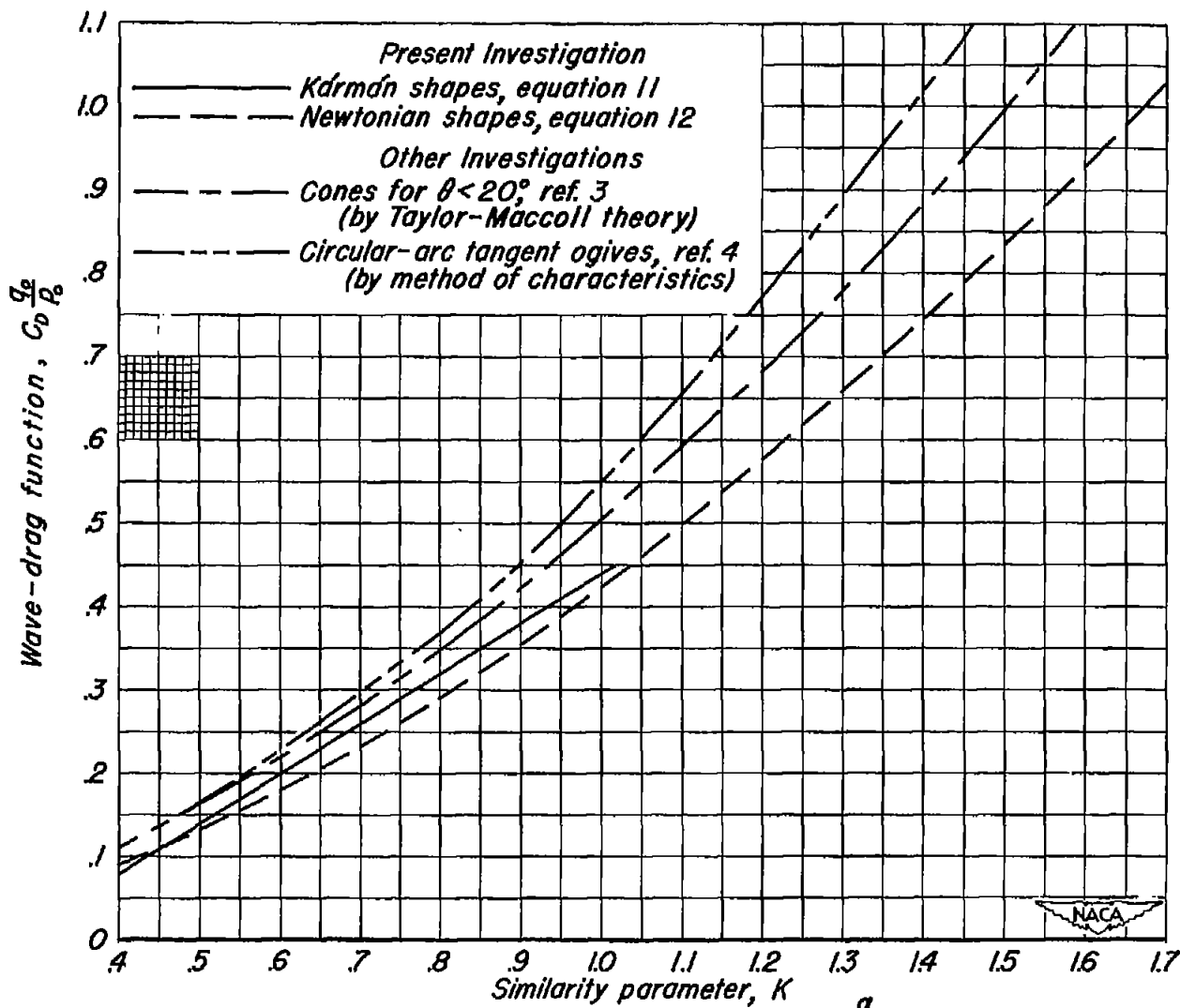


Figure 9- Comparison of the theoretical variations of wave-drag function $C_D \frac{g_0}{p_0}$ with similarity parameter K for various shapes.